S1 OFR transfer functions

The OFR transfer functions were defined as linear combinations of Taylor distributions:

$$E(t) = \sum_i \frac{f_i}{2} \exp\left(-\frac{\mathrm{Pe}_i\,(\tau_i - t)^2}{4\tau_i t}\right)\sqrt{\frac{\mathrm{Pe}_i}{\pi\tau_i t}}, \tag{S1}$$

where

$$\sum_i f_i = 1. \tag{S2}$$

We used a combination of two Taylor distributions for DOFR and three for PAM. The parameters for calculating the transfer functions for different OFRs are shown in Table S1.

The standard deviation of the transfer function reflects the transfer function broadness. Because the transfer function is analogous to a probability density function, its standard deviation (σ) is defined as

$$\sigma = \sqrt{\int_0^\infty (t - \tau_{mean})^2\, E(t) dt}, \tag{S3}$$

where τ_{mean} is the mean residence time defined as

$$\tau_{mean} = \int_0^\infty t E(t) dt. \tag{S4}$$

The standard deviation was calculated numerically by first calculating the values of the transfer function with Eq. S1, then calculating the mean residence time with Eq. S4 and finally obtaining the standard deviation with Eq. S3. The upper limit of integration was 700 s.

S2 Effect of chemical kinetics on SOA response

In the analysis, it is assumed that all SOA precursors get oxidized in the OFRs (Sect. 3). In other words, the square pulse of any SOA precursor is assumed to produce a SOA mass concentration profile at the OFR outlet that is similar to a CO_2 profile produced by a square pulse injection of CO_2. This assumption can be written as

$$[SOA]_1(t) = ([VOC]_0 * E)(t) \cdot y, \tag{S5}$$

where y is the SOA yield, E is the transfer function of CO_2 and $[VOC]_0$ is the time-dependent precursor (volatile organic compound) concentration at the OFR inlet. A more advanced approach considers that the formation of SOA depends on the amount of precursor gas that is oxidized by OH radicals, as discussed in Sect. 3. This can be written as

$$[SOA]_2(t) = \Delta[VOC](t) \cdot y = (([VOC]_0 * E)(t) - [VOC]_f(t)) \cdot y, \tag{S6}$$

where $[VOC]_f$ is the precursor concentration at OFR outlet. Assuming the precursor reacts only with OH radicals, its concentration at OFR outlet is

$$[VOC]_f(t) = ([VOC]_0 * E)(t) \cdot \exp(-k \cdot [OH]_{avg} \cdot t), \tag{S7}$$

where k is the reaction rate constant between the precursor and OH radical and $[OH]_{avg}$ is the average OH radical concentration in the OFR. Note that Eq. S7 is applicable only for a short input pulse of precursor gas. The average OH radical concentration is defined as

$$[OH]_{avg} = \frac{OH_{exp}}{\tau_{mean}}, \tag{S8}$$

where OH_{exp} is the average OH exposure in the OFR. The average OH exposure is a measurable quantity that can be determined by measuring the decay of an OH reactive substance in the OFR (e.g. Barmet et al. (2012)). For a steady input of precursor gas, the product $[OH]_{avg} \cdot t$ in Eq. S7 should be replaced with the average OH exposure.

For toluene SOA production in DOFR the basic approach (Eq. S5) led to a satisfactory agreement with the experimental data (Fig. S1a), with very little difference to the more accurate approach (Eq. S6) because almost all toluene is consumed by OH radicals even at the shorter residence times. For PAM (Fig. S1c), the difference between the two simulations is higher because the fraction of sample that spends the least time in the reactor has too low OH exposure to oxidize all toluene. The SOA formation by Eq. S6 in Fig. S1 is calculated by assuming an average OH exposure of $7.9 \cdot 10^{11}$ $\mathrm{cm^{-3}\ s^{-1}}$, since this was the average OH exposure in the toluene experiment shown in Fig. S1a.

The effect of chemical kinetics is higher for precursor gases that react slower with OH radicals. The reaction rate constant of toluene is $5.63 \cdot 10^{-12}$ $\mathrm{cm^3\ s^{-1}}$, whereas the reaction rate constant of benzene, another common anthropogenic precursor, is smaller, $1.22 \cdot 10^{-12}$ $\mathrm{cm^3\ s^{-1}}$ (Atkinson and Arey, 2003). Figures S1b and S1d show that the assumption in Eq. S5 is invalid for benzene.

The applicability of the assumption in Eq. S5 in general depends on the composition of precursor gases in the vehicle exhaust. According to VOC data presented by Timonen et al. (2017) for gasoline vehicle exhaust in cold-start phase, the average reaction rate constant of the measured aromatic VOCs weighted by their mass concentration was $9.08 \cdot 10^{-12}$ $\mathrm{cm^3\ s^{-1}}$. Since this value is higher than the toluene reaction rate constant, we consider the assumption in Eq. S5 sufficient to model SOA formation in gasoline vehicle exhaust for the purposes of this work, as long as the average OH exposure in the reactor is approximately $7.9 \cdot 10^{11}$ $\mathrm{cm^{-3}\ s^{-1}}$ or higher.

Additionally, all the aromatic VOCs listed by Atkinson and Arey (2003) except benzene, toluene and tert-butylbenzene have higher reaction rate constants than toluene. Regarding the precursor gases in diesel exhaust, all the intermediate volatile organic compounds in diesel vehicle exhaust that were speciated by Zhao et al. (2015) have higher reaction rate constants than toluene.

S3 Deconvolution

The deconvolved signal ($[C]^*(t)$) was calculated by using a non-linear programming solver *fmincon* (Matlab R2021b). The solver tries to find the non-negative signal that, when convolved with the OFR transfer function, results in minimal sum of

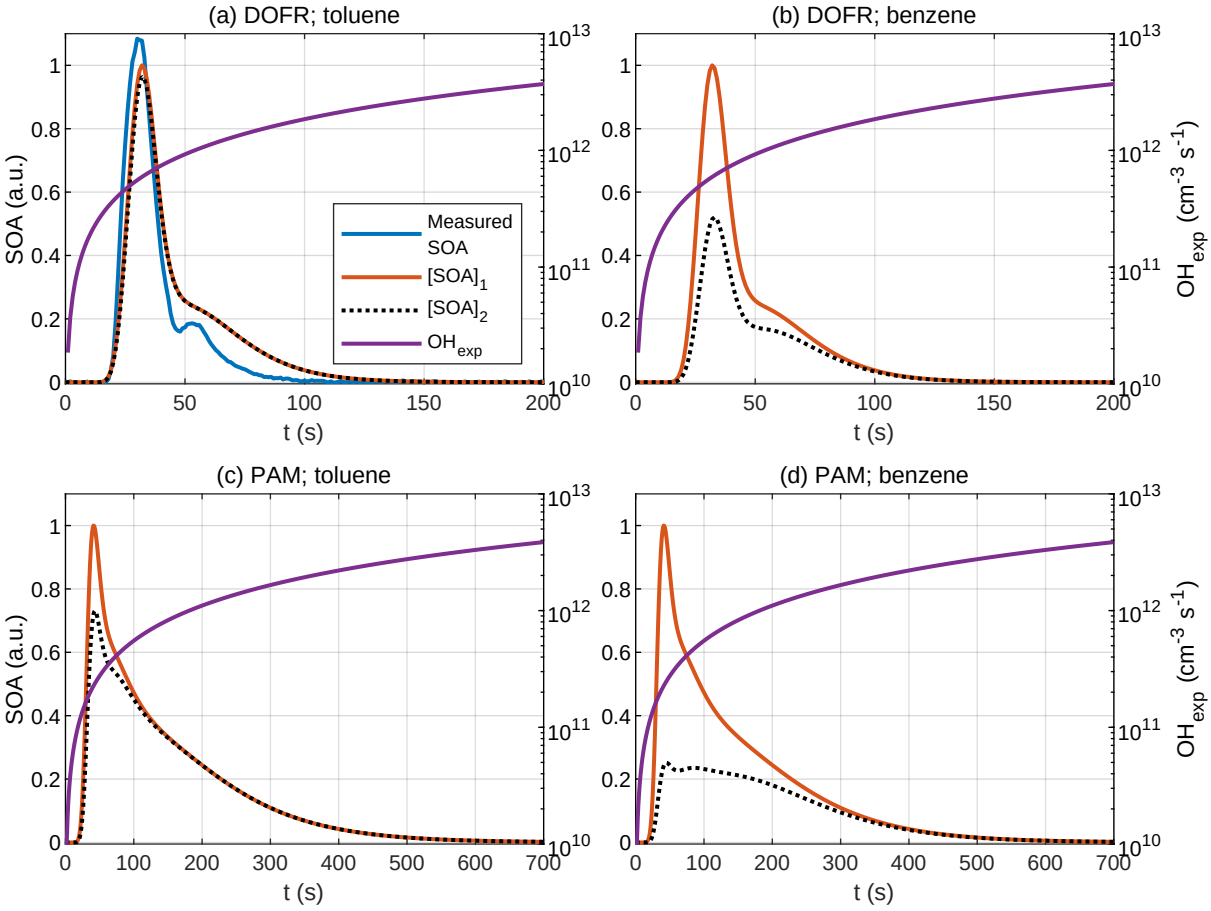

Figure S1. Measured SOA (downstream of the internal ejector diluter, dilution ratio 8.5) with 'low UV' setting compared to SOA modeled with Eq. S5 ($[SOA]_1$) and with Eq. S6 ($[SOA]_2$) (a), where $[VOC]_0$ is a convolved 10 s square pulse of toluene, and y is the SOA yield determined from steady input experiments. Toluene concentration upstream DOFR during the pulse was 398 ppb, measured from a steady input experiment. The square pulse was convolved with CO_2 transfer function. Average flow rate was 6.0 slpm. All concentrations are normalized to the maximum value of $[SOA]_1$. The model results are shown also for benzene SOA formation in DOFR (b) as well as for toluene (c) and benzene (d) in PAM reactor. The OH exposure shown in the right y axis corresponds to the OH exposure experienced by the VOC exiting the reactor at time t. Even though the average OH exposure of the sample (VOC + air) measured at OFR outlet is constant, the OH exposure experienced by the VOC is time-dependent in case of pulse injection.

residual squares. In other words, the solver tries to find $[C]^*(t)$, for which $\sum\left(\left([C]^* * E\right)(t) - [C]_{OFR}(t)\right)^2$ is smallest, where $[C]^*(t) \geq 0$ and $[C]_{OFR}(t)$ is the SOA concentration measured downstream of the OFR. For all deconvolution cases presented here, the solver converged to an optimal solution.

S4 Synthetic driving cycles

Examples of synthetic driving cycles are shown in Fig. S17. The synthetic driving cycles were generated with the following algorithm:

1) The cycle length is is a random value between 240 s and 2400 s with uniform probability distribution.

2) The vehicle type is either Diesel or Gasoline with equal probabilities. The vehicle type affects the behaviour of $\mathrm{CO_2}$ concentration in step 2 of $\mathrm{CO_2}$ concentration algorithm.

Exhaust flow rate:

1) Choose whether the engine is on or off (can be off when measuring hybrid engine vehicles). The probability for engine off condition is 0.01.

2a) If the engine is off, choose a random value between 10 s and 600 s for the duration of engine off period. The exhaust flow rate is zero during the engine off period. Start a new period at the end of this period and define the next period by moving back to step 1.

2b) If the engine is on, choose whether the period of constant value for exhaust flow rate is a stable period (duration between 25 s and 100 s) or a short period (duration between 2 s and 25 s). The probability for a stable period is 0.1 and the probability for duration is uniformly distributed in the specified range.

3) Choose a random number between $0.75 \cdot 10^{-3}$ and $0.08\ \mathrm{m^3\ s^{-1}}$ as the constant value for the exhaust flow rate for this period. The probability is uniformly distributed in this range.

4) Assign the new value for the period by generating a smooth transition between the previous value and the new value with Eq. S9.

5) Start a new period following this period and define the next period by moving back to step 1. Repeat the steps until the end of the cycle is reached.

$\mathrm{CO_2}$:

1) Choose whether the period of constant value for $\mathrm{CO_2}$ concentration is a stable period (duration between 25 s and 100 s) or a short period (duration between 2 s and 25 s). The probability for a stable period is 0.1 and the probability for duration is uniformly distributed in the specified range.

2) Choose the constant value of $\mathrm{CO_2}$ for this period. If the vehicle type is Diesel, the probability follows truncated normal distribution between 1 and 14% with mean of 7% and variance of 6%. If the vehicle type is Gasoline, the probability follows truncated normal distribution between 3 and 14% with mean of 13% and variance of 2%. These parameters reflect the fact that the $\mathrm{CO_2}$ concentration in gasoline exhaust is close to constant because the engines typically operate at constant air-to-fuel ratio, whereas in the diesel engines, the air-to-fuel ratio is load dependent.

3) Assign the concentration value for this period by generating a smooth transition between the previous value and the new value with Eq. S9.

4) Start a new period following this period and define the next period by moving back to step 1. Repeat the steps until the end of the cycle is reached.

5) For all engine off periods that were defined when assigning the engine exhaust flow rate, assign CO_2 concentration of 0%. This simulates a sampling system where the OFR is always sampling zero air when the engine is off.

Hydrocarbons:

1) Choose whether the period of constant value for HC concentration is a stable period (duration between 25 s and 100 s) or a short period (duration between 2 s and 25 s). The probability for a stable period is 0.1 and the probability for duration is uniformly distributed in the specified range.

2) Choose the constant value of HC for this period. The HC value is either low (0-10 ppm), medium (15-200 ppm) or high (500-4000 ppm), reflecting the observed concentrations in cold- and hot-start NEDC for the measured gasoline vehicle. The probability is 0.513 for low concentration, 0.48 for medium concentration and 0.007 for high concentration. In case of low concentration, the probability follows truncated normal distribution between 0 and 10 ppm with mean of 1 ppm and variance of 10 ppm. In case of medium concentration, the probability follows truncated normal distribution between 15 ppm and 200 ppm with mean of 30 ppm and variance of 60 ppm. In case of high concentration, the probability follows truncated normal distribution between 500 and 4000 ppm with mean of 1000 ppm and variance of 1000 ppm.

3) Assign the concentration value for this period by generating a smooth transition between the previous value and the new value with Eq. S9.

4) Start a new period following this period and define the next period by moving back to step 1. Repeat the steps until the end of the cycle is reached.

5) For all engine off periods that were defined when assigning the engine exhaust flow rate, assign HC concentration of 0 ppm. This simulates a sampling system where the OFR is always sampling zero air when the engine is off.

A smooth transition between two different values is generated with the following equation:

$$[C](t) = \frac{[C]_0 e^{3 \cdot 1.5} + [C]_f e^{1.5 \cdot t}}{e^{3 \cdot 1.5} + e^{1.5 \cdot t}}, \tag{S9}$$

where $[C]_0$ is the previous value and $[C]_f$ is the new value.

Table S1. Parameters for calculating OFR transfer functions.

Reactor	DOFR						PAM
Gas	CO_2			Toluene			CO_2
UV lamps	off	low	high	off	low	high	on
f_1	0.3301	0.5438	0.2429	0.4799	0.5877	0.1391	0.1357
f_2	0.6699	0.4562	0.7571	0.5201	0.4123	0.8609	0.3098
f_3	-	-	-	-	-	-	0.5545
Pe_1	70.2468	59.9304	185.0773	34.5126	40.2907	249.9402	31.8016
Pe_2	13.7971	13.9073	9.3947	13.4908	24.6792	11.7453	9.8594
Pe_3	-	-	-	-	-	-	6.5239
τ_1 (s)	24.7862	27.1867	18.7578	31.1628	28.3984	22.1192	33.7762
τ_2 (s)	37.3938	49.9008	34.9837	47.5170	54.6086	37.5168	59.6120
τ_3 (s)	-	-	-	-	-	-	159.0658

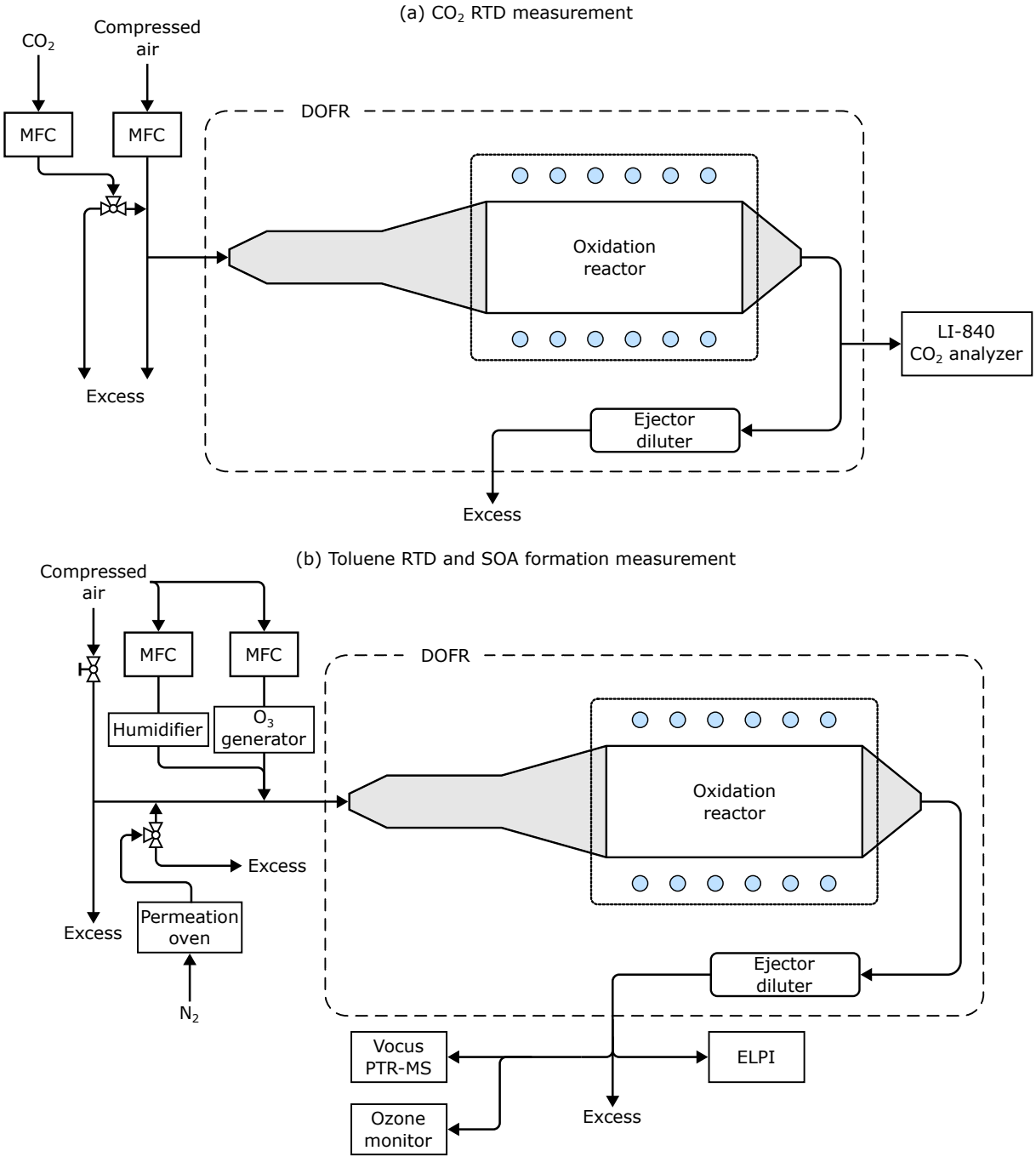

Figure S2. The measurement setup (DOFR dimensions not to scale). The blue circles depict the DOFR UV lamps. The flows were controlled with mass flow controllers (MFCs; Alicat Scientific). The ozone was generated with an UV lamp (Model 1000, Jelight Company Inc.) and measured with Model 205 analyzer (2B Technologies).

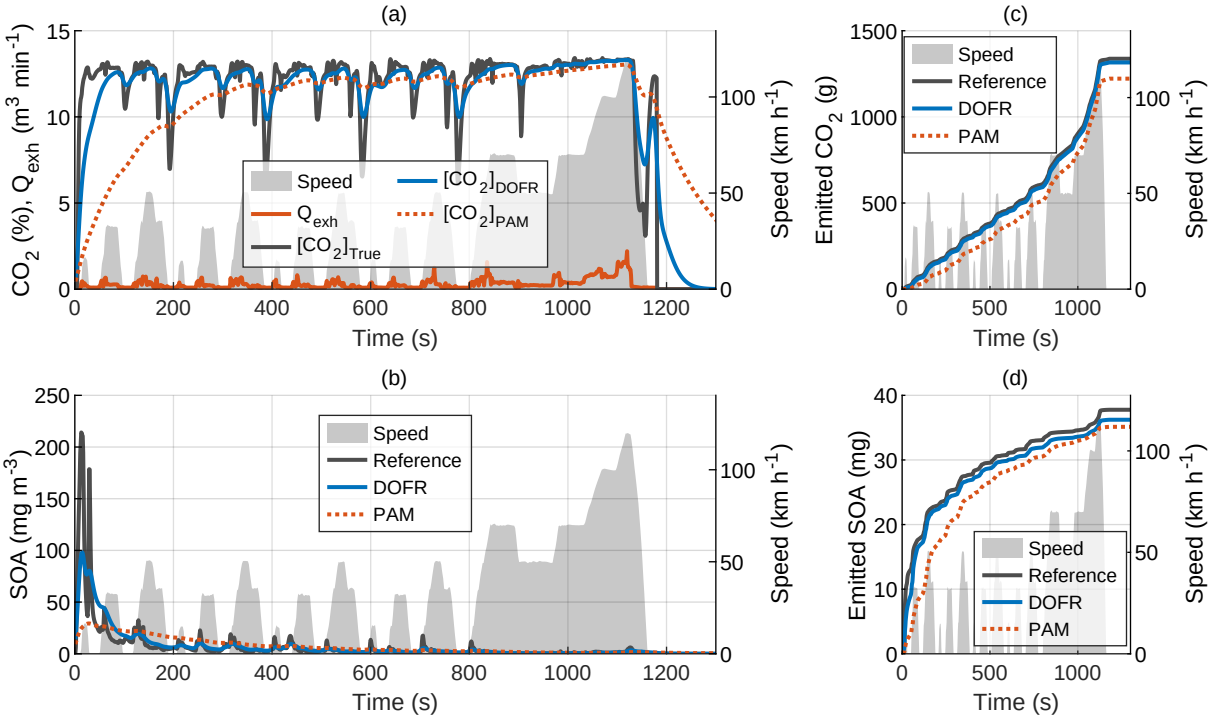

Figure S3. Time series of exhaust flow rate (Q_{exh}), tailpipe and OFR outlet concentrations of CO_2 (a) and SOA (b) in cold-start NEDC, and the cumulative emissions of CO_2 (c) and SOA (d). The OFR data is simulated based on tailpipe concentrations and OFR transfer functions, and the SOA concentration refers to HC concentration multiplied with Y. All OFR data is delay corrected.

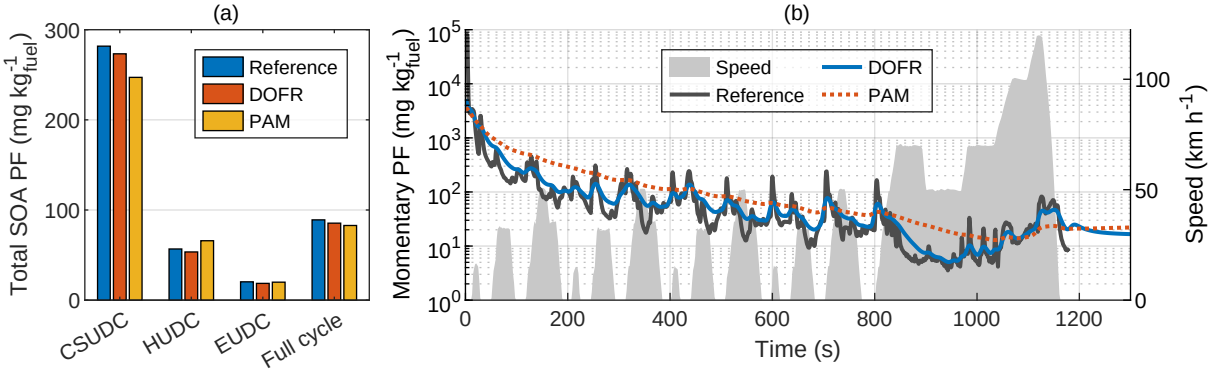

Figure S4. Total SOA PFs of subcycles and full driving cycle (a), and time series of reference SOA PF and SOA PFs determined from OFR measurements (b) in cold-start NEDC. The integrated SOA PF in panel (a) is calculated by normalizing the SOA emission to true CO_2 emission, whereas for the momentary SOA PF in panel (b), the SOA concentration is normalized to OFR CO_2 concentration. The PFs in both panels are calculated for semi-synthetic SOA data that is linearly proportional to the measured HC concentration in the tailpipe. CSUDC, HUDC and EUDC represent approximately 400 s subcycles within the full cycle. Note logarithmic axis scale in panel (b).

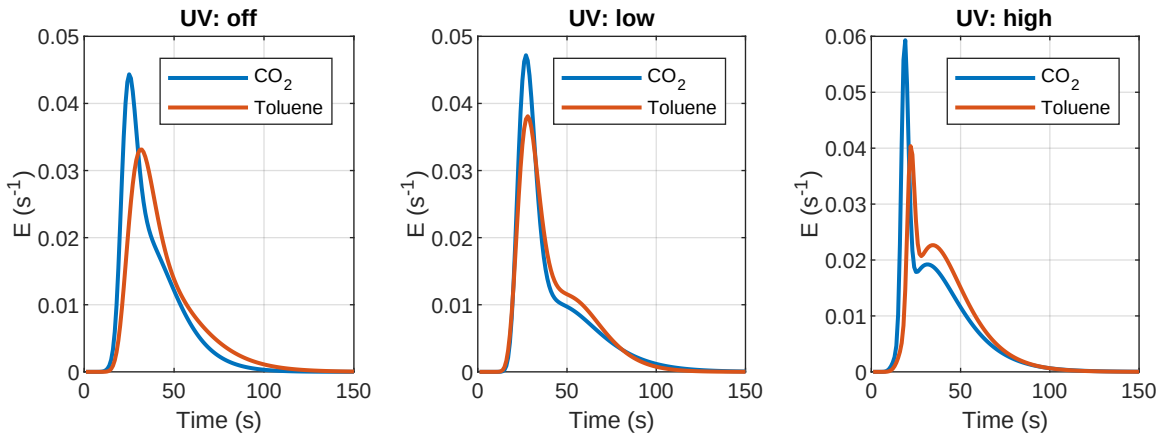

Figure S5. DOFR transfer functions for CO_2 and toluene with different UV lamp settings. Mean flow rate was 6.8 slpm for CO_2 experiments and 6.0 slpm for toluene experiments. According to Dekati, the the transfer function of the current DOFR model consists of a single peak instead of the double peak observed here with the prototype model when the UV lamps were on.

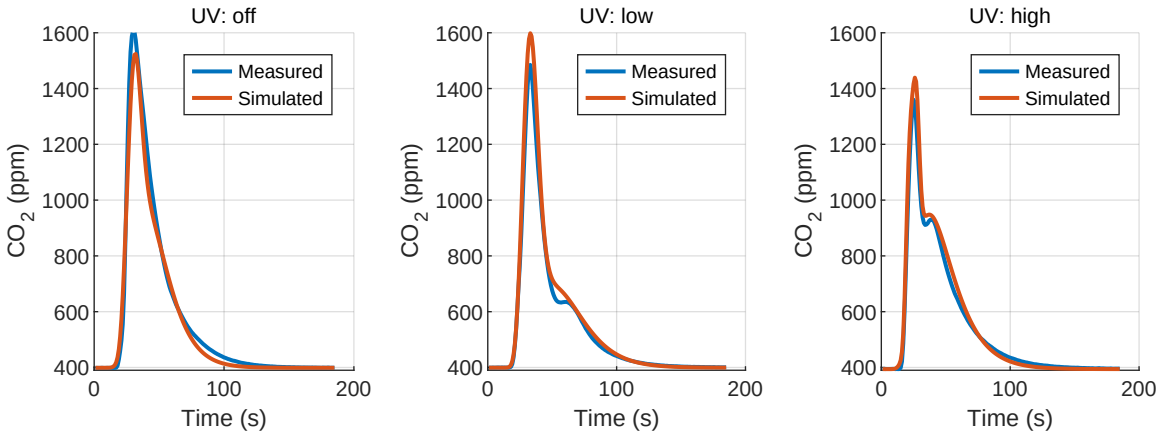

Figure S6. The measured DOFR output for 10 s input pulses of CO_2 and the simulated output, which is a 10 s square pulse convolved with the transfer function corresponding to the UV setting.

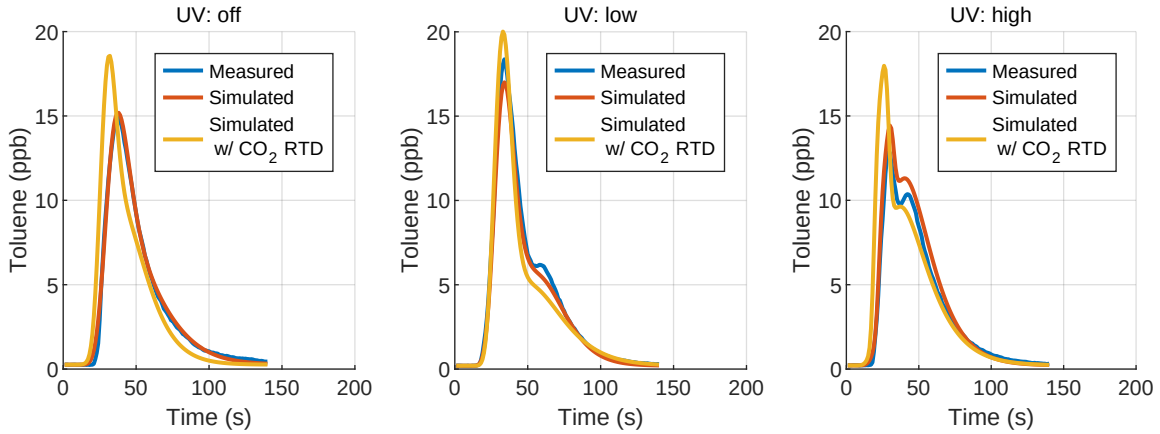

Figure S7. The measured DOFR output for 10 s input pulses of toluene and the simulated output, which is a 10 s square pulse convolved with either the CO_2 or toluene transfer function corresponding to the UV setting.

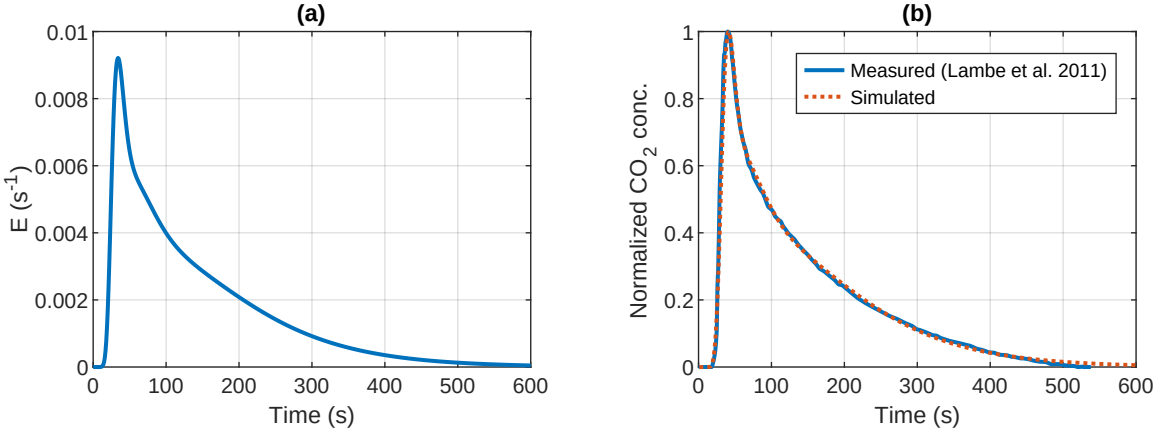

Figure S8. Best fit transfer function for PAM (a), and a 10 s square pulse of CO_2 convolved with the transfer function (b). The experimental data origins from measurements by Lambe et al. (2011), where the PAM UV lamps were on and the ring flow was used.

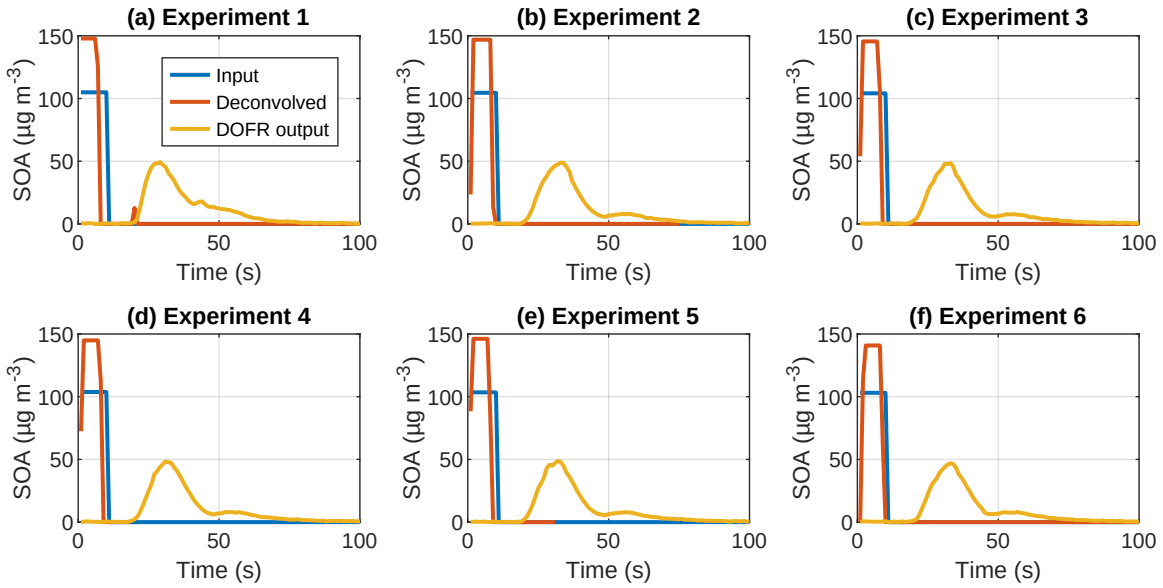

Figure S9. Deconvolution performance test for 6 repetitions of a 10 s toluene pulse input with 'low UV' setting. DOFR output is the actual SOA mass measured with ELPI downstream the internal ejector diluter (dilution ratio 8.5). Input is the square pulse of toluene multiplied with the SOA yield (determined from steady-state experiments) and divided by the dilution ratio. Deconvolved is the result of deconvolution of DOFR output (using CO_2 transfer function). Deconvolution overestimates the peak height and underestimates the duration. This is probably because the CO_2 transfer function does not perfectly represent the SOA formation dynamics, as observed in Fig. S1a.

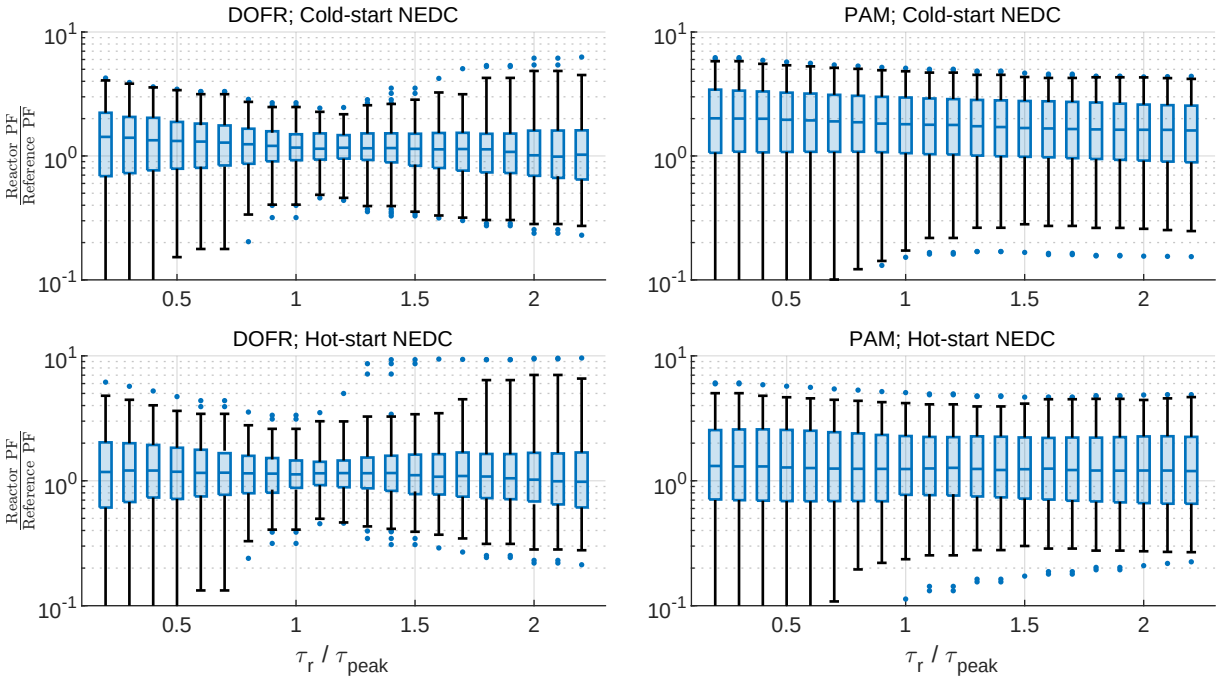

Figure S10. The ratio of OFR PF to reference PF when using standard calculation method with different delay correction constants (τ_r). The PFs are calculated for 10 s bins in the driving cycles and different delay correction constants are normalized to τ_{peak}.

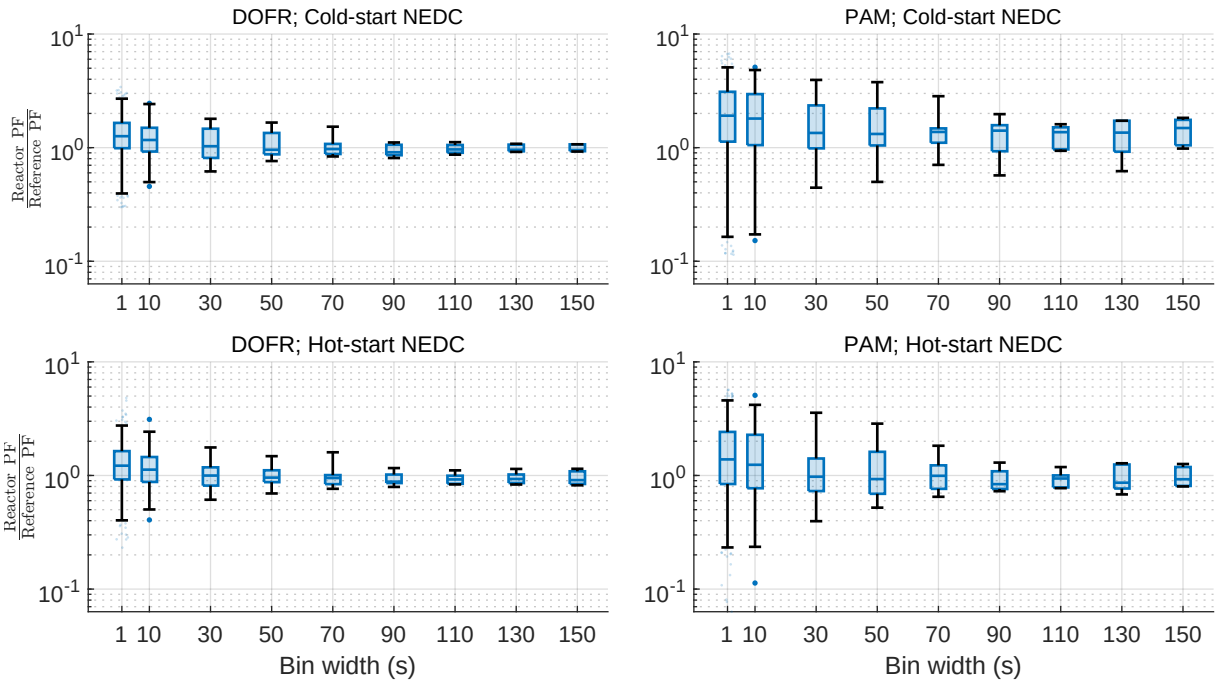

Figure S11. The effect of calculation bin duration on OFR PF accuracy for hot-start and cold-start NEDC.

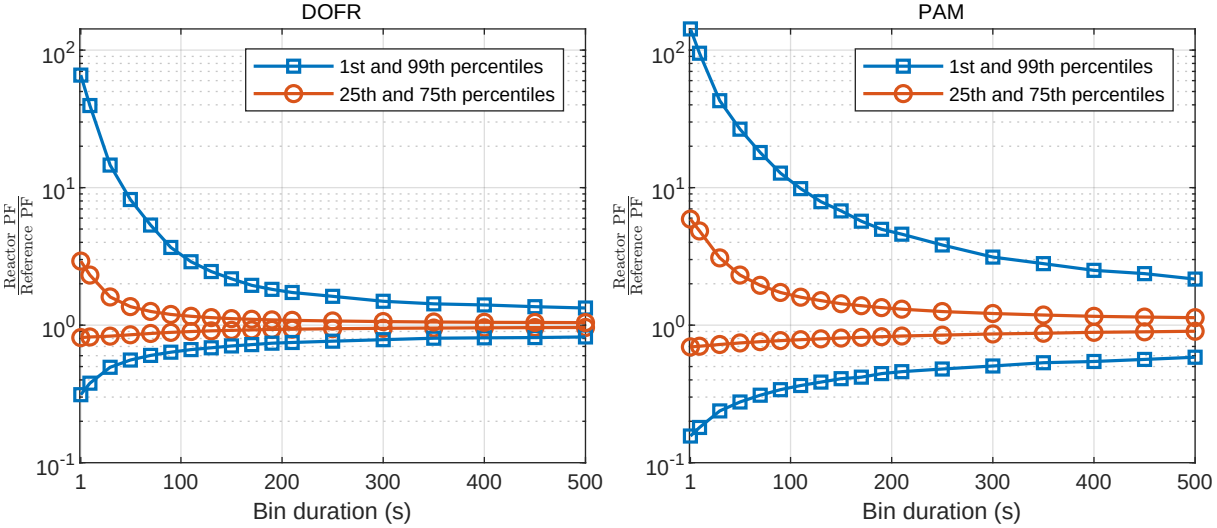

Figure S12. The effect of calculation bin duration on OFR PF accuracy for 10000 synthetic driving cycles.

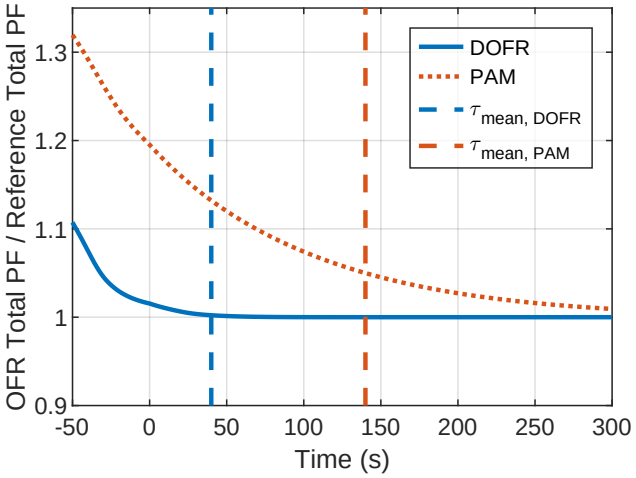

Figure S13. Comparison of OFR total PF to the reference PF, when using CVS method (Eq. 11) and sampling zero air after the cycle ends. The driving cycle here is cold NEDC, and the cycle ends at 0 s. The mean residence times of the OFRs (τ_{mean}) are shown with dashed lines. The data is not corrected for OFR delay, as this is not necessary for the CVS method when calculating the full cycle PF. In contrast, the delay correction will result in some error in the full cycle PF.

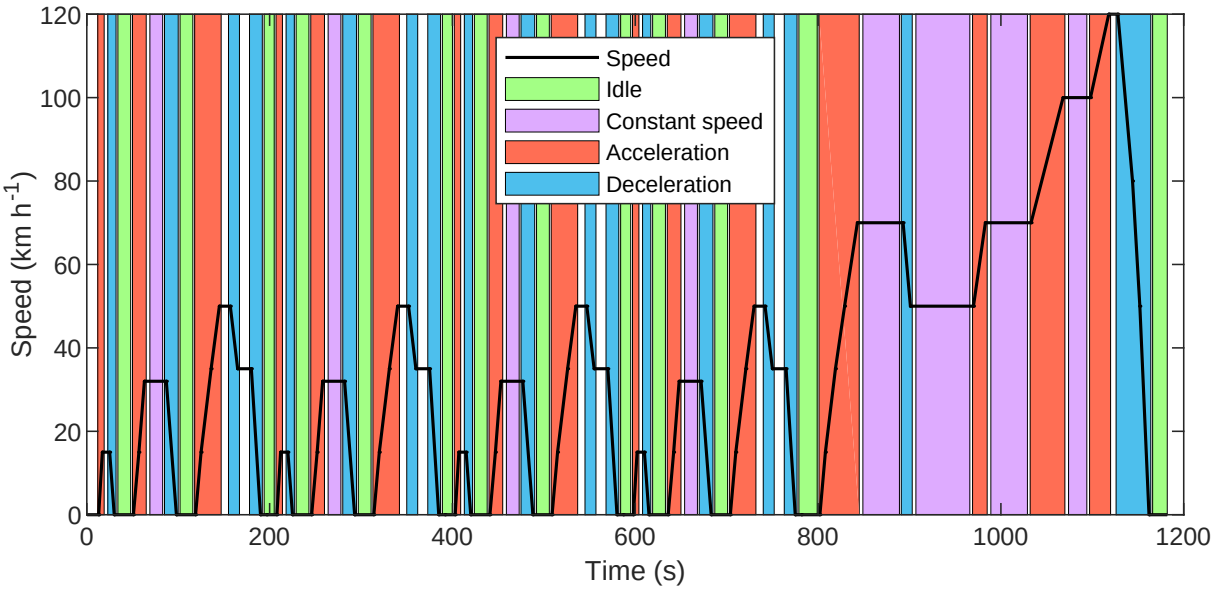

Figure S14. NEDC divided into bins representing different driving conditions.

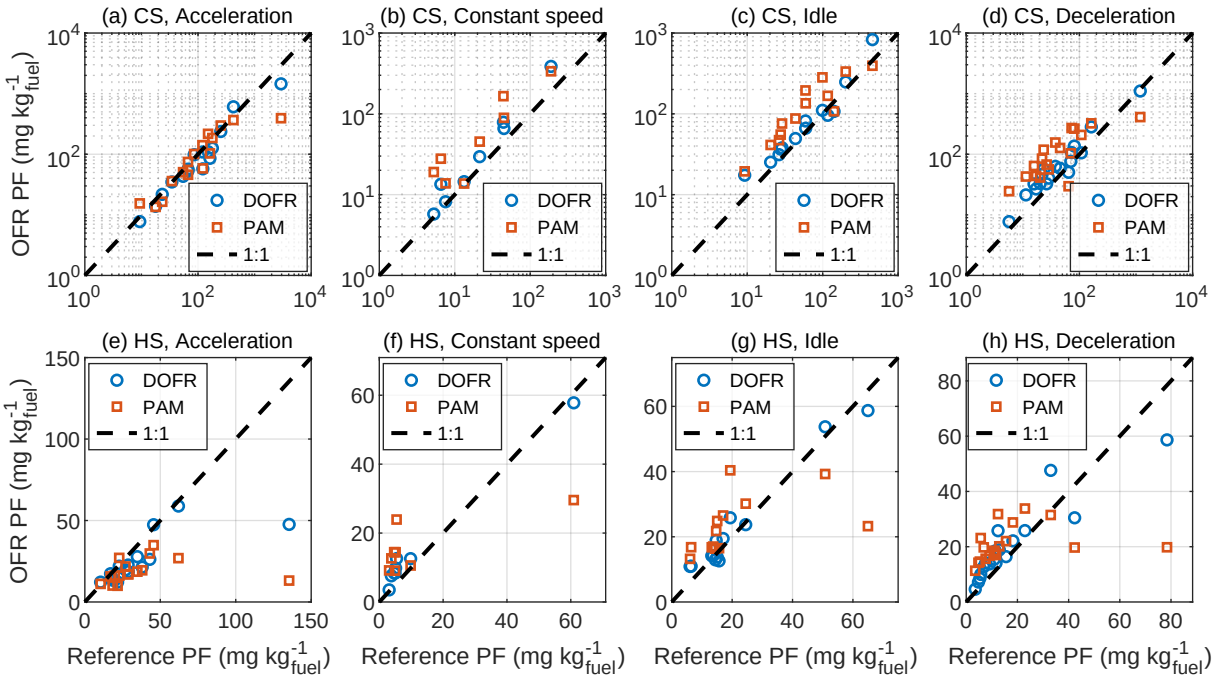

Figure S15. Correlations between OFR PFs and reference PFs using the standard PF calculation method. The data corresponds to the histograms in Fig. 4. Note the logarithmic scale in panels (a)-(d).

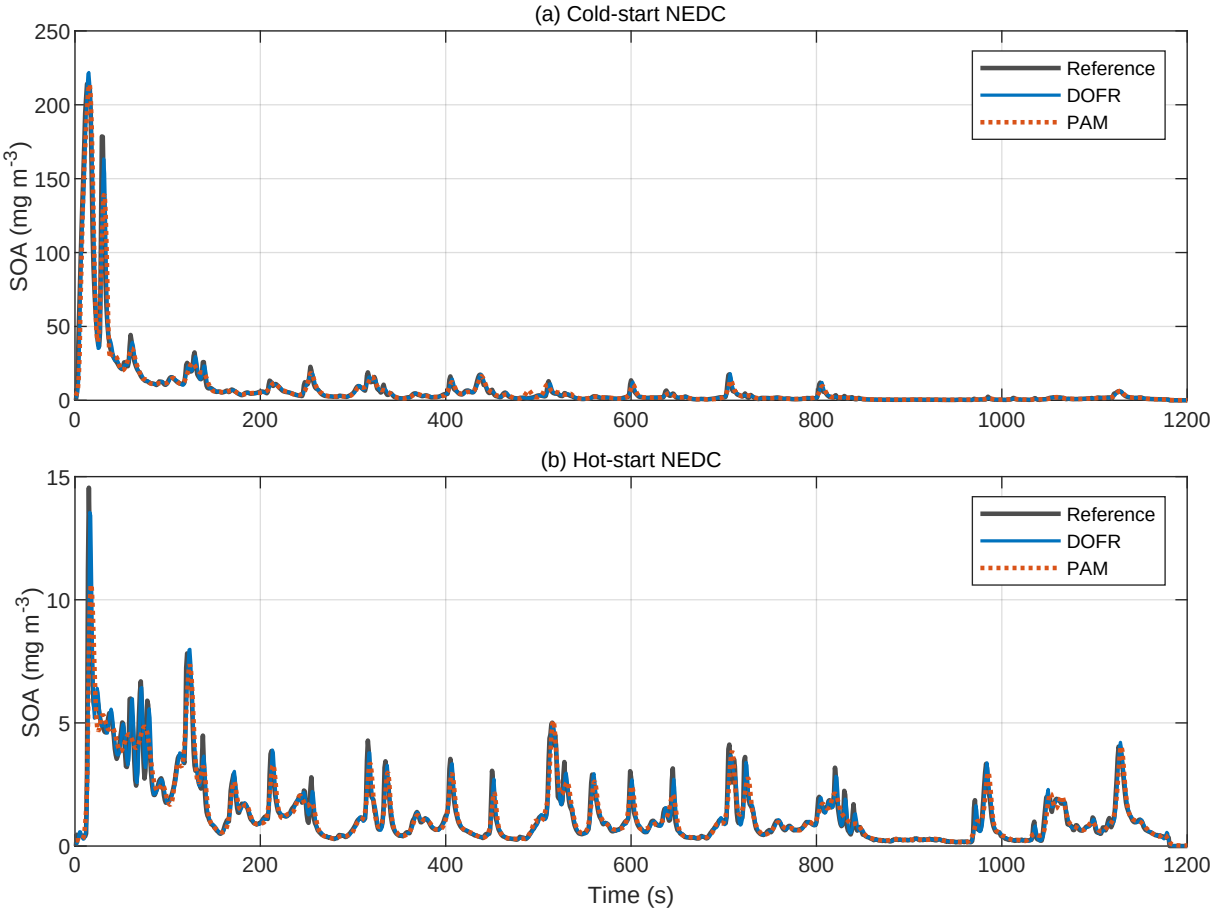

Figure S16. Reference SOA concentration ($[HC] \cdot Y$) compared to deconvolved OFR SOA signals. For OFRs, the product $[HC] \cdot Y$ is first convolved with the OFR transfer function and then deconvolved using the same transfer function.

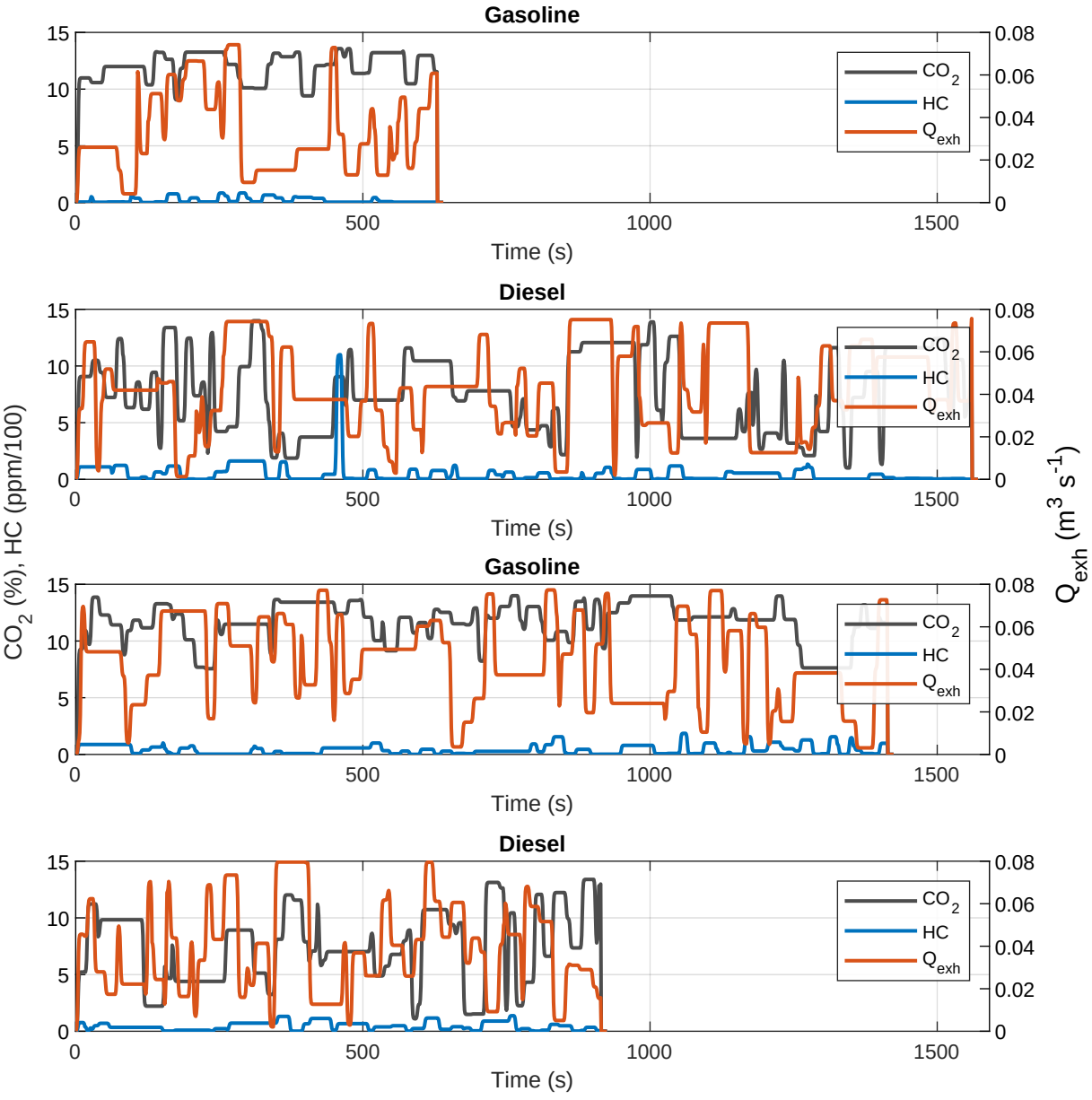

Figure S17. Examples of synthetic driving cycles generated with the algorithm described in Sect. S4.

References

Atkinson, R. and Arey, J.: Atmospheric degradation of volatile organic compounds, Chemical reviews, 103, 4605–4638, 2003.

Barmet, P., Dommen, J., DeCarlo, P., Tritscher, T., Praplan, A., Platt, S., Prévôt, A., Donahue, N., and Baltensperger, U.: OH clock determination by proton transfer reaction mass spectrometry at an environmental chamber, Atmospheric Measurement Techniques, 5, 647–656, 2012.

Lambe, A. T., Ahern, A. T., Williams, L. R., Slowik, J. G., Wong, J. P. S., Abbatt, J. P. D., Brune, W. H., Ng, N. L., Wright, J. P., Croasdale, D. R., Worsnop, D. R., Davidovits, P., and Onasch, T. B.: Characterization of aerosol photooxidation flow reactors: heterogeneous oxidation, secondary organic aerosol formation and cloud condensation nuclei activity measurements, Atmospheric Measurement Techniques, 4, 445–461, https://doi.org/10.5194/amt-4-445-2011, 2011.

Timonen, H., Karjalainen, P., Saukko, E., Saarikoski, S., Aakko-Saksa, P., Simonen, P., Murtonen, T., Dal Maso, M., Kuuluvainen, H., Bloss, M., Ahlberg, E., Svenningsson, B., Pagels, J., Brune, W. H., Keskinen, J., Worsnop, D. R., Hillamo, R., and Rönkkö, T.: Influence of fuel ethanol content on primary emissions and secondary aerosol formation potential for a modern flex-fuel gasoline vehicle, Atmospheric Chemistry and Physics, 17, 5311–5329, 2017.

Zhao, Y., Nguyen, N. T., Presto, A. A., Hennigan, C. J., May, A. A., and Robinson, A. L.: Intermediate Volatility Organic Compound Emissions from On-Road Diesel Vehicles: Chemical Composition, Emission Factors, and Estimated Secondary Organic Aerosol Production, Environmental Science & Technology, 49, 11 516–11 526, https://doi.org/10.1021/acs.est.5b02841, 2015.